



RESEARCH ARTICLE

Podoplanin is dispensable for mineralized tissue formation and maintenance in the Swiss outbred mouse background

Masako Toda Nakamura^{1,2}  | Honghao Zhang¹ | Dayong Guo³ | Hiroki Ueharu¹ | Haichun Pan¹ | Greg Scott⁴ | Marie Harris^{3,5} | Manas Ray⁴ | Jiang Q. Feng^{3,6} | Stephen E. Harris^{3,5} | Lynda F. Bonewald^{3,7} | Yuji Mishina¹ 

¹Department of Biologic and Materials Sciences & Prosthodontics, School of Dentistry, University of Michigan, Ann Arbor, Michigan, USA

²Section of Pediatric Dentistry, Department of Oral Growth and Development, Fukuoka Dental College, Fukuoka, Japan

³Department of Oral Biology, School of Dentistry, University of Missouri-Kansas City, Kansas City, Missouri, USA

⁴Knock Out Core, National Institute of Environmental Health Sciences, National Institutes of Health, Research Triangle Park, North Carolina, USA

⁵UT Health San Antonio, Graduate School of Biomedical Sciences, San Antonio, Texas, USA

⁶Department of Biomedical Sciences, Texas A&M College of Dentistry, Dallas, Texas, USA

⁷Indiana Center for Musculoskeletal Health and Department of Anatomy, Cell Biology and Physiology, Indiana University, Indianapolis, Indiana, USA

Correspondence

Yuji Mishina, Department of Biologic and Materials Sciences & Prosthodontics, University of Michigan, School of Dentistry, 1011 N. University Avenue, Ann Arbor, MI 48109-1078.
Email: mishina@umich.edu

Funding information

Fukuoka Dental College Foreign Exchange Program; National Institutes of Health, Grant/Award Number: P30AR069620; National Institutes of Health, Grant/Award Numbers: P01AG39355, R01DE024797, R03DE027456, R01DE020843

Summary

Podoplanin, PDPN, is a mucin-type transmembrane glycoprotein widely expressed in many tissues, including lung, kidney, lymph nodes, and mineralized tissues. Its function is critical for lymphatic formation, differentiation of type I alveolar epithelial lung cells, and for bone response to biomechanical loading. It has previously been shown that *Pdpm* null mice die at birth due to respiratory failure emphasizing the importance of *Pdpm* in alveolar lung development. During the course of generation of *Pdpm* mutant mice, we found that most *Pdpm* null mice in the 129S6 and C57BL6/J mixed genetic background die at the perinatal stage, similar to previously published studies with *Pdpm* null mice, while all *Pdpm* null mice bred with Swiss outbred mice survived. Surviving mutant mice in the 129S6 and C57BL6/J mixed genetic background showed alterations in the osteocyte lacunocanalicular network, especially reduced osteocyte canaliculi in the tibial cortex with increased tibial trabecular bone. However, adult *Pdpm* null mice in the Swiss outbred background showed no overt differences in their osteocyte lacunocanalicular network, bone density, and no overt differences when challenged with exercise. Together, these data suggest that genetic variations present in the Swiss outbred mice compensate for the loss of function of PDPN in lung, kidney, and bone.

KEYWORDS

craniofacial development, exercise, osteocyte, Podoplanin, skeletogenesis, tooth bud

1 | INTRODUCTION

Podoplanin (PDPN), also known as E11, gp38, RTI40, or T1 alpha, is a mucin-type transmembrane glycoprotein widely expressed in many tissues such as lung, kidney, lymph nodes, and mineralized tissues (Astarita, Acton, & Turley, 2012; Schulze, Witt, Kasper, Lowik, & Funk, 1999). PDPN is extensively O-glycosylated with a high content of sialic acid (Gonzalez & Dobbs, 1998). PDPN interacts with a variety of intracellular and transmembrane proteins to mediate effects on cell migration and adhesion (Prideaux, Loveridge, Pitsillides, & Farquharson, 2012). Binding of PDPN to CD44 or ezrin/radixin/moesin (ERM) proteins results in increased cell migration and rearrangement of the actin cytoskeleton to generate actin-rich protrusions of the membrane (Martin-Villar et al., 2010; Prideaux et al., 2012). PDPN is thought to be involved in the development and homeostatic maintenance of several kinds of cells and tumorigenesis (Renart et al., 2015; Retzbach et al., 2018; Suzuki-Inoue, Osada, & Ozaki, 2017).

Pdgn is expressed in osteocytes and osteoblasts (Zhang et al., 2006), choroid plexus (Zhang et al., 2006), perineurium (Noda, Amano, Hata, Kojima, & Sawa, 2010), tooth germ epithelial cells (Imaizumi, Amano, Tsuruga, Kojima, & Sawa, 2010), salivary gland myoepithelium (Amano, Imaizumi, Kaji, Kojima, & Sawa, 2011), thymus type I epithelial cells, prostate myofibroblasts, follicular dendritic cells, and immature cells such as fetal germ cells and developing Sertoli cells. *Pdgn* is expressed by budding *Prox1*-positive lymphatic progenitor cells around embryonic day 11, E11.0 (Schacht et al., 2003). *Pdgn* null mice die at birth because of respiratory failure associated with reduced numbers of differentiated type I alveolar epithelial cells in the lung (Ramirez et al., 2003). The expression of *Pdgn* is also restricted to *Prox1*-positive lymphatic endothelial cells of the lymph sac (Grogger et al., 2004; Schacht et al., 2003). Lack of *Pdgn* leads to alterations in the final patterning of the lymphatic vasculature as well as in lymph transport. *Pdgn* null mice also have defects in lymphatic formation with diminished lymphatic transport and congenital lymphedema (Schacht et al., 2003).

Pdgn is expressed in craniofacial tissues, for example, tongue, bone, muscle, and tooth (Imaizumi et al., 2010; Noda et al., 2010; Sawa, Iwasawa, & Ishikawa, 2008; Zhang et al., 2006). Within bones, PDPN is only found in the dendritic processes of osteocytes, and not found in osteoblasts in vivo (Bonewald, 2011; Zhang et al., 2006). These studies also show that PDPN is localized within osteocyte membranes and at punctate vesicles at the interface between osteocytes and uncalcified osteoid cells (Schulze et al., 1999; Zhang et al., 2006). Expression of *Pdgn* in the dendritic processes of osteocytes is increased in response to mechanical strain in vitro (Zhang et al., 2006). PDPN is also found in enamel epithelia (Sawa et al., 2008), odontoblasts (Imaizumi et al., 2010), and cementocytes (N. Zhao et al., 2016). PDPN expression and location suggest roles in skeletogenesis and craniofacial development. Indeed, conditional deletion of *Pdgn* in bone cells using *Osteocalcin*-Cre results in a significant reduction in dendrite volume and length in association with improved biomechanical properties such as resistance to higher fracturing load (Staines et al., 2017). These transgenic mice also showed resistance against load-induced osteoarthritis and ovariectomy induced osteoclast activation (Staines et al., 2019; Staines et al., 2020), demonstrating important roles of PDPN in bone strength and function.

During the course of generation and analyses of *Pdgn* mutant mice where loxP insertion resulted in hypomorphs (Prideaux et al., 2015), we discovered that neonatal lethality varies depending on genetic background. Despite a high mortality rate for homozygous mutant mice for the floxed allele of *Pdgn* in a mixed background of 129S6 and C57BL6/J (129/B6), all survived when bred with Swiss outbred mice twice. In this report, we examined possible skeletal phenotypes in surviving mice in the 129/B6 mixed background and in the Swiss outbred background to identify potential functions of PDPN in skeletogenesis.

2 | MATERIALS AND METHODS

2.1 | Mouse breeding and genotyping

Generation of the podoplanin (*Pdgn*) mutant allele was reported previously (Prideaux et al., 2015). In brief, one loxP was inserted into the 5'-UTR of the exon 1 and the other loxP was inserted into the first intron (Figure S1, Supporting Information). Details of the initial screening strategy of targeted embryonic stem cells (AB2.2 and UG347 lines) and subsequent genotyping strategy using PCR are summarized in Figure S1. After removal of the neo cassette by crossing with Flipper mice (Farley et al., 2000), we set up breeding between *Pdgn^{fl/+}* mice and *Pdgn^{fl/+};Ocn-Cre* mice to disrupt *Pdgn* in the osteoblast lineage (M. Zhao et al., 2002). Later, heterozygous mice (*Pdgn^{fl/+}*) were bred with *Sox2-Cre* transgenic mice (Hayashi et al., 2003) to remove the floxed region to inactivate gene function (Cre-recombined allele, designated “-” hereafter). Homozygous mice for the Cre-recombined allele (*Pdgn^{-/-}*) were generated by intercrossing of the Cre-recombined heterozygous mice. Noon of the date when the vaginal plug observed was designated as E0.5. Genotypes were determined by PCR analyses; primers A and B were used to amplify fragments from wildtype (187 bp) and the *Pdgn* floxed alleles (292 bp for fx). Primers C and B were used to detect presence of the neomycin selection cassette (400 bp). Primers D and B were used to detect Cre-dependent deletion of the floxed region (348 bp for “-”) (Figure S1). Sequences for genotyping primers are: A (5'-CCCTAACACCCCCCTCCGC-3'), B (5'-CCTCTTCAGGTCTATCCCCAGCC-3'), C (5'-ACCGACTCAGCACATTCC-3'), D (5'-ATAAATGCCGACTGTGCCGAGAGG-3'). The mutations are maintained in a mixture of 129S6 and C57BL6/J. In some cases, the mutant mice were backcrossed twice or more with Swiss Webster outbred mouse stock (Taconic). All mouse experiments were performed in accordance with institutional guidelines covering the humane care and use of animals in research. The animal protocols were approved by the Institutional Animal Care and Use Committees at the National Institute of Environmental Health Sciences, the University of Missouri at Kansas City, and the University of Michigan.

2.2 | Quantification of *Pdgn* gene expression

Approximately 100 mg of tissue was collected from lung, intestines, kidney, and bone of 3-month-old male mice followed by total RNA

extraction using TRIzol Reagent, catalog number 15596-026 (Invitrogen, Carlsbad, CA), according to the manufacturer's instructions. Reverse transcription was performed with 100 ng of total RNA using the High Capacity cDNA Reverse Transcription Kit, catalog number 4368814 (Applied Biosystems, Foster City, CA). Real time polymerase chain reaction (PCR) was conducted with TaqMan Gene Expression Assays designed for mouse *E11/gp38*, catalog number 4331182 (Applied Biosystems). TaqMan Rodent GAPDH Control Reagents, catalog number 4308313 (Applied Biosystems) was used as an internal control. Quantitative PCR was conducted on an ABI Prism 7000 Sequence Detection System (Applied Biosystems) following the manufacturer's instructions. The final expression level of *Pdpr* mRNA was normalized as a ratio to the GAPDH mRNA level from the same sample.

2.3 | Histology, skeletal staining, and immunocytochemistry

Embryos or adult tissue was fixed in 4% paraformaldehyde (PFA), dehydrated, and embedded in paraffin. Seven micrometer sections were cut and stained with hematoxylin and eosin (H&E), Picrosirius red or Von Kossa according to standard procedures. For immunodetections, embryos or adult tissues were fixed in 4% PFA at 4°C overnight followed by incubation in 20% sucrose/PBS at 4°C for overnight, embedded in O.C.T. compound (Sakura Finetek, Tokyo, Japan), and serially sectioned in 10 µm. The samples were incubated with hamster anti-Podoplanin (1:100 dilution, sc-53533, Santa Cruz Biotechnology, Santa Cruz, CA), goat anti-Amelogenin (1:100 dilution, sc-365284, Santa Cruz Biotechnology), at 4°C overnight. Alexa Fluor 488 goat Anti-Syrian Hamster IgG or Alexa Fluor 488 goat anti-mouse IgG1 (1:100 dilution, A21121, Invitrogen) were used as secondary antibodies. For kidney and lung, serially sectioned paraffin sections were incubated with an E11 antibody against Podoplanin (1:100 dilution, a kind gift from Dr. Andrew Farr) and subsequently incubated with a peroxidase-conjugated goat anti-Syrian hamster IgG (sc-2905, Santa Cruz Biochemistry) then color developed using a DAB substrate kit (Vector Laboratories). For bones, Cy3 goat anti-hamster IgG (Jackson ImmunoResearch Laboratories, 107-165-142) was used for detection. For liver analyses, the following antibodies were used: CD90, which specifically marks Hepatic progenitor cells: AB3105 (Abcam), Rat antibody, Anti-Rat-Alexa fluor 488; Albumin: MAB 1455 (R & D system), Mouse antibody, Anti-Mouse-Alexa fluor 595, and E11, Sc53533 (Santa Cruz Biochemistry), Hamster antibody, Anti-Hamster-Alexa fluor 488. Sections were mounted with ProLong Gold antifade reagent with DAPI (P36935, Invitrogen). Intensity of fluorescent signal was quantified using ImageJ 1.53J.

2.4 | Scanning electron microscopy and Osteoimaging

Samples were first fixed in 70% ethanol for 3 days and then transferred to 100% ethanol to dehydrate under vacuum overnight. Next,

they were put into 10 mL infiltration solution (methylmethacrylate 8.5 mL, dibutylphthalate 1.4 mL, polyethylene glycol 400,100 µL, and benzoyl peroxide 70 mg) and shaken at room temperature for 4 days. Ten milliliter embedding solution (methylmethacrylate 8.5 mL, dibutylphthalate 1.4 mL, polyethylene glycol 400,100 µL, and benzoyl peroxide 400 mg) was prepared in a glass vial on ice. N, N-dimethyl-p-toluidine, 33 µL added as an accelerator into the vial, and the samples were then placed in the vial followed by purging with nitrogen. The vials were tightly capped and kept at 4°C until polymerization was complete. Embedded samples were trimmed and polished to expose the bone surface, then cleaned with a sonicating machine. Phosphoric acid (37%) was used to etch the surface for 10 s, followed by bleaching with 5% sodium hypochlorite for 5 min. After washing and air drying, the surface was coated with palladium and gold, and examined under a Philips SEM 515 scanning electron microscope in the secondary electron mode.

The scanning electron microscopy (SEM) images of acid etched bone surfaces revealed the configuration of the lacuno-canalicular network in bone. Four images were taken from each sample. The distances between an osteocyte and its three nearest neighbors were measured, averaged, and compared between the control and mutant bones. The density of canaliculi was determined at a site which is 10 µm beneath the endosteal surface of cortical bone at the mid-shaft of both the ulna and tibia, and 1–2 mm below the proximal growth plate in the trabecular bone of the tibia.

2.5 | microCT analyses

Tibias from 3-month-old male mice were analyzed using a µCT 40 X-ray machine (Scanco Medical, Southwestern, PA) with a resolution of 15 µm and a threshold of 300 Hounsfield units. Cortical total volume, cortical bone volume, cortical thickness, cortical apparent density of bone and marrow, cortical material density of bone were measured at the mid-shaft (–1 to +1 mm). Trabecular bone volume/total volume, trabecular number, trabecular thickness, trabecular apparent density of bone and marrow, and trabecular material density of bone were measured at 1 to 2 mm below the growth plate.

2.6 | Exercise on treadmill

Four-month-old males and females ($n = 4$ for each gender, $n = 4$ for *Pdpr*^{+/+} or *Pdpr*^{-/-}) were exercised for 3 weeks. Each exercise session lasted 30 min and the average speed was 12 m/min at a 5° incline (Iura et al., 2015). One day after the end of the exercise regime, at 5 months of age, all the mice were euthanized, and femora were removed.

2.7 | Statistical analysis

One-way analysis of variance with Bonferroni's posttest was used to conduct statistical comparisons among multiple groups. If there were

only two groups, unpaired two-tailed *t*-test was used. The threshold for statistical significance was set to be $p < 0.05$. All computations were performed with GraphPad Prism version 3.0 (GraphPad Software, San Diego, CA).

3 | RESULTS

3.1 | The floxed *Pdpn* allele is highly hypomorphic resulting in an abnormal osteocyte morphology

Floxed mice were generated in a 129S6/C57BL6 background (129/B6) through homologous recombination in embryonic stem cells (Figure S1). Homozygous mice for the floxed allele showed perinatal lethality due to lung malfunction (Table 1). While homozygous mice for the floxed allele (*Pdpn*^{fl/fl}) were present in the Mendelian ratio at

E18.5, the expected number of homozygous mice was drastically reduced at the 3 weeks of age. Removal of the neo-cassette from the locus did not improve the lethality on the 129/B6 background (Table 1). We speculate this is probably due to the insertion of the 5' loxP site into a 5'UTR region of exon 1 compromising expression of *Pdpn* (Figure S1). This concept was supported by the observations that levels of *Pdpn* mRNA from 1 month old tibia, kidney, and lung of the homozygous mice for the floxed allele are below detection (Figure 1a-c). mRNA levels in the heterozygous tissues were significantly reduced, but PDPN proteins was detected by immunohistochemistry at comparable intensity to wild type, while no signal was observed in the homozygous tissues (Figure 1d).

We took an advantage of the tissue-specific gene disruption strategy to disrupt endogenous *Pdpn* using an *Osteocalcin-Cre* (*Ocn-Cre*), which is expressed in late osteoblasts to early osteocytes (M. Zhao et al., 2002) to insure ablation of *Pdpn* in the osteoblast lineage, in order

Background	Stage	Wildtype (%) <i>Pdpn</i> ^{+/+}	het (%) <i>Pdpn</i> ^{fl/+}	Homo (%) <i>Pdpn</i> ^{fl/fl}	Total	Resorption site
129/B6 ^{\$}	3 weeks	29 (22.7)	58 (72.0)	6 (5.3)	93	n/a
129/B6	3 weeks	17 (31.2)	54 (62.3)	4 (6.5)	75	n/a
129/B6	E18.5	15 (21.4)	34 (48.6)	21 (30.0)	70	0
Swiss ^{&}	3 weeks	18 (37.0)	19 (47.8)	21 (15.2)	81	n/a
Swiss [#]	3 weeks	25 (36.8)	30 (44.1)	13 (19.1)	68	n/a
Swiss [#]	E18.5	13 (22.4)	31 (53.4)	14 (24.1)	58	n/a

TABLE 1 Ratio of genotyping of offspring from the breeding between *Pdpn* floxed het mice

Abbreviations: \$, floxed allele with the neo cassette; &, backcrossed one time; #, backcrossed twice.

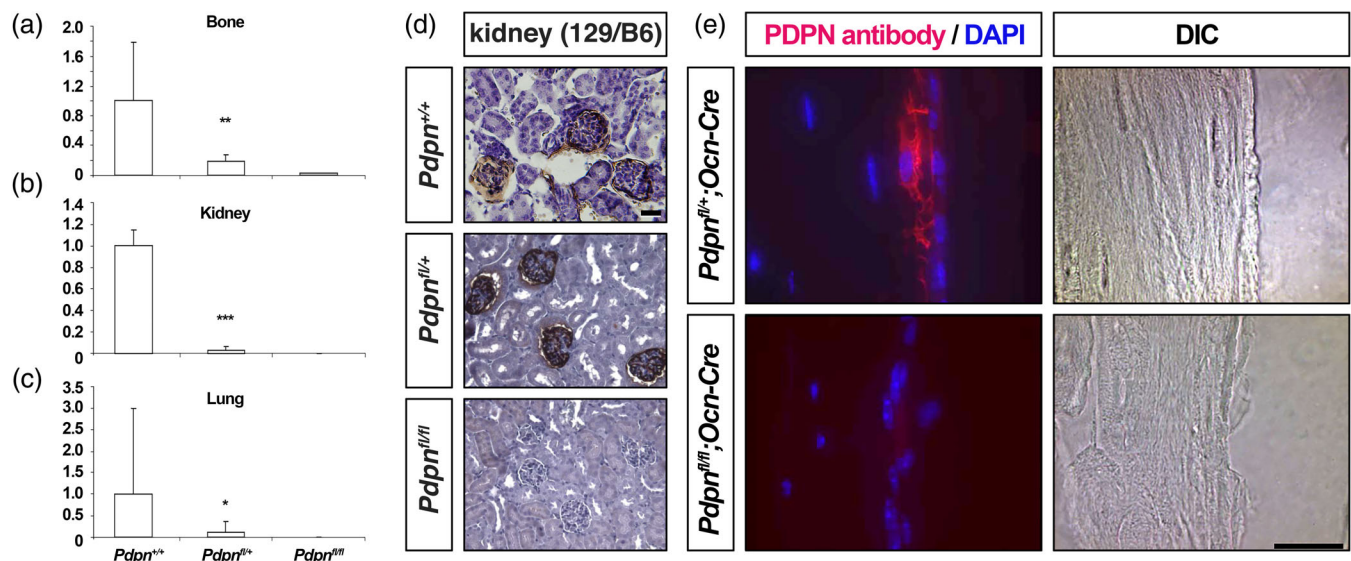


FIGURE 1 The floxed *Pdpn* allele in 126S6/C57BL6 mixed background showed a significantly reduced *Pdpn* expression. (a-c) Quantitative real time PCR for *Pdpn* expression. Data were collected from femur (a), kidney and (b) lung (c) of 3-month-old male mice. Sample sizes were 3, 7, and 1 for (*Pdpn*^{+/+}), heterozygous (*Pdpn*^{fl/+}), and homozygous (*Pdpn*^{fl/fl}) mice, respectively. The neomycin selection cassette was removed before setting up intercross of the heterozygous mice. Error bars are SDs. (d) Presence of PDPN were detected using sections from kidney of 129S6 and C57BL6/J mixed background (129/B6). Bar = 20 μ m. (e) Immunostaining for PDPN on vertebral sections (Cy3, red). The newly embedded osteocyte close to the bone surface was stained positive in the controls. The sections were counterstained with DAPI in blue. Differential interference contrast (DIC) of the same view is shown on the right. The Scale bar = 20 μ m. $N = 2$ for controls, $n = 2$ for mutants

to investigate potential bone phenotypes of the surviving mutant mice in 129/B6 background. While heterozygous mice for the floxed allele of *Pdpr* (*Pdpr^{fl/+};Ocn-Cre*) showed detectable immunosignal of PDPN especially in areas of newly embedded osteocytes, no signal was observed level in bones from *Pdpr^{fl/fl};Ocn-Cre* mice. (Figure 1e).

Among the limited number of surviving mice at 3-months of age (*Pdpr^{fl/fl};Ocn-Cre*), there were two classes of mutant mice: normal sized with normal appearance ($n = 4$) and smaller size with ascites ($n = 2$) (Figure 2a). The normal appearing mutant mice displayed alterations in the lacunocanalicular network in the cortex of their tibia (Figure 2b, c). The number of canaliculi was reduced to half, while no significant change in the average distance between the three nearest neighboring osteocytes was observed (Figure 2d, e). The microCT analyses revealed a significantly higher volume in the trabecular compartment of the tibia (Figure 2f). This is mainly due to an increase in trabecular number resulting in an increase of apparent density in the

mutant bones. Cortical compartments did not show significant differences between two genotypes (Figure 2g).

3.2 | *Pdpr* does not play a role in embryonic mineralized tissue development

After removal of the floxed segment of *Pdpr* to generate a Cre-recombined allele (=functionally null, designated “-” hereafter) (Figure 3a), we set up intercrosses between heterozygous mutant mice for the Cre-recombined allele. As expected, *Pdpr^{-/-}* mice died soon after birth showing impaired formation of alveolar airspace (Figure 3b) resembling the previously reported phenotype found in homozygous *Pdpr* mutant mice deficient in exon 1 (Ramirez et al., 2003). For possible skeletal phenotypes, we investigated calvaria, tibial growth plate and metaphysis. Histologic observation of

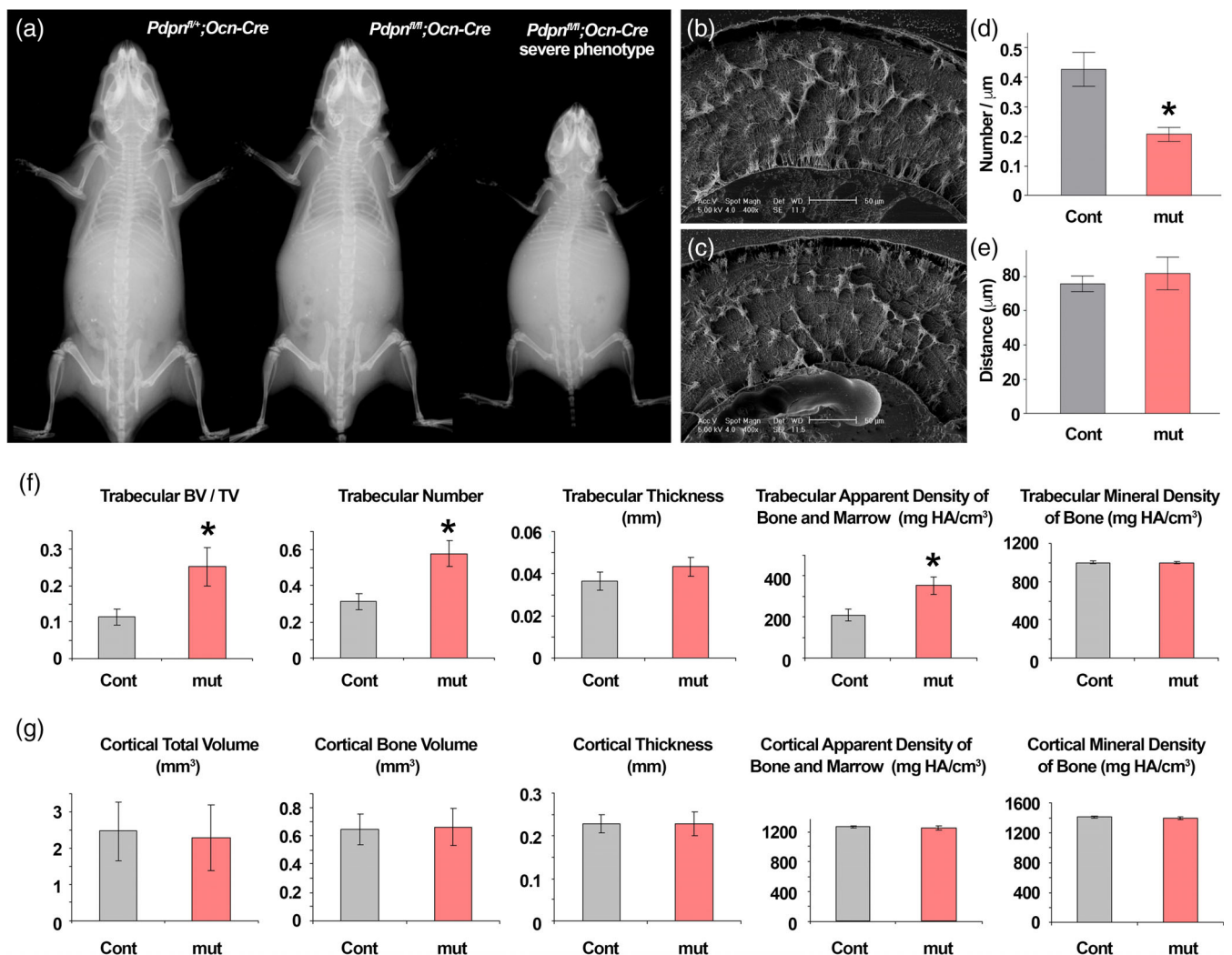


FIGURE 2 Surviving homozygous mice for the floxed *Pdpr* allele in 126S6/C57BL6 mixed background showed a reduced canalicular number with increased bone volume. (a) X-ray radiographs of *Pdpr^{fl/+};Ocn-Cre* (control, Cont) and *Pdpr^{fl/fl};Ocn-Cre* (mutant, mut) mice at 3-month after birth. (b, c) Acid-etched scanning electron micrograms of control (b) and mutant (c) tibia. Bar = 50 μm . (d, e) Measurements of lacuno-canalicular network. (f, g) microCT measurements of bone parameters in the trabecular compartment (f) and cortical compartment (g) of tibia. $N = 4$ for controls, $n = 3$ for mutants

H&E-stained sections did not show overt changes in these bones (Figure 3c). Osteoblasts and osteocytes were present in *Pdpr*^{-/-} mice similar to controls. Since *Pdpr* is highly expressed in early osteocytes

(Zhang et al., 2006), we examined mineral deposition and collagen maturation to determine potential functional changes of osteoblasts and osteocytes. By Picrosirius Red staining, there were no significant

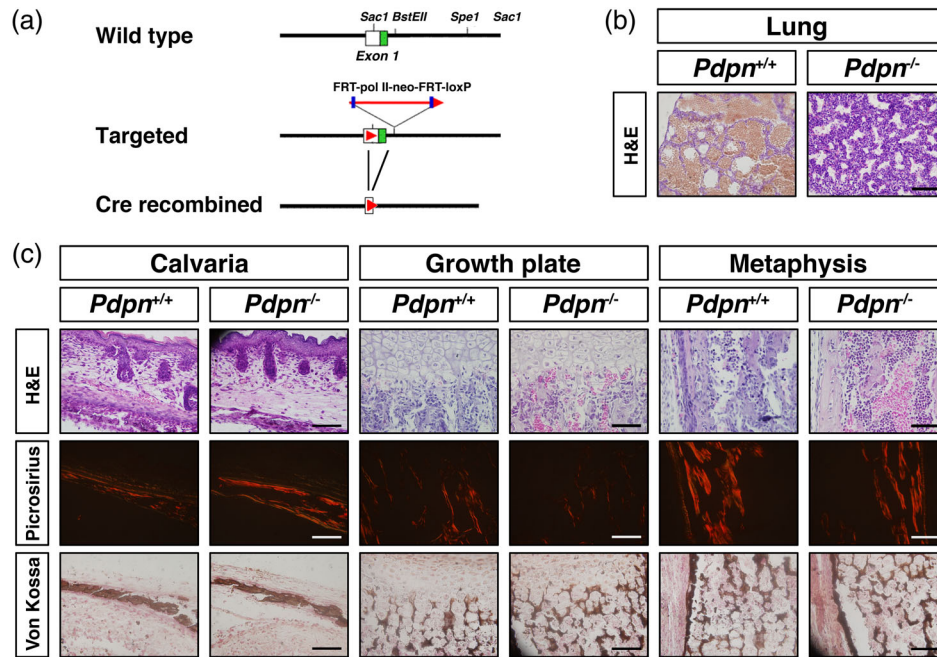


FIGURE 3 *Pdpr* mutant mice have no overt abnormalities in bones. (a) Conversion of the *Pdpr*-floxed allele to a Cre-recombined allele. After confirmation of correct gene targeting event in embryonic stem cells and subsequent germ line transmission as detailed in Figure S1, mice heterozygous for *Pdpr* floxed allele with a Pkg-neo cassette (*Pdpr*^{fl/+}) were bred with Flipper mice (Farley et al., 2000) to remove the neo cassette (*Pdpr*^{fl/+}). The *Pdpr*^{fl/+} mice also were bred with Sox2-Cre mice (Hayashi et al., 2003) to delete exon 1 to generate a recombined null allele (*Pdpr*^{-/-}). (b) Histologic observation of newborn stage lung. *Pdpr*^{-/-} lungs characteristically show dense cellularity, narrow and tortuous air spaces, and thicker interalveolar septae compared to littermate control lungs. Paraffin sections (7 μ m) stained with H&E. Bar = 50 μ m. (c) Histologic observations of calvaria, tibial growth plate, and metaphysis at E18.5. Paraffin sections (7 μ m) were stained with H&E (upper), Picrosirius red (middle), or Von Kossa (lower). *Pdpr*^{-/-} mice showed similar phenotypes of soft tissue, chondrocytes, mature collagen fiber, and calcified bone matrix with those found in littermate controls. Bar = 50 μ m

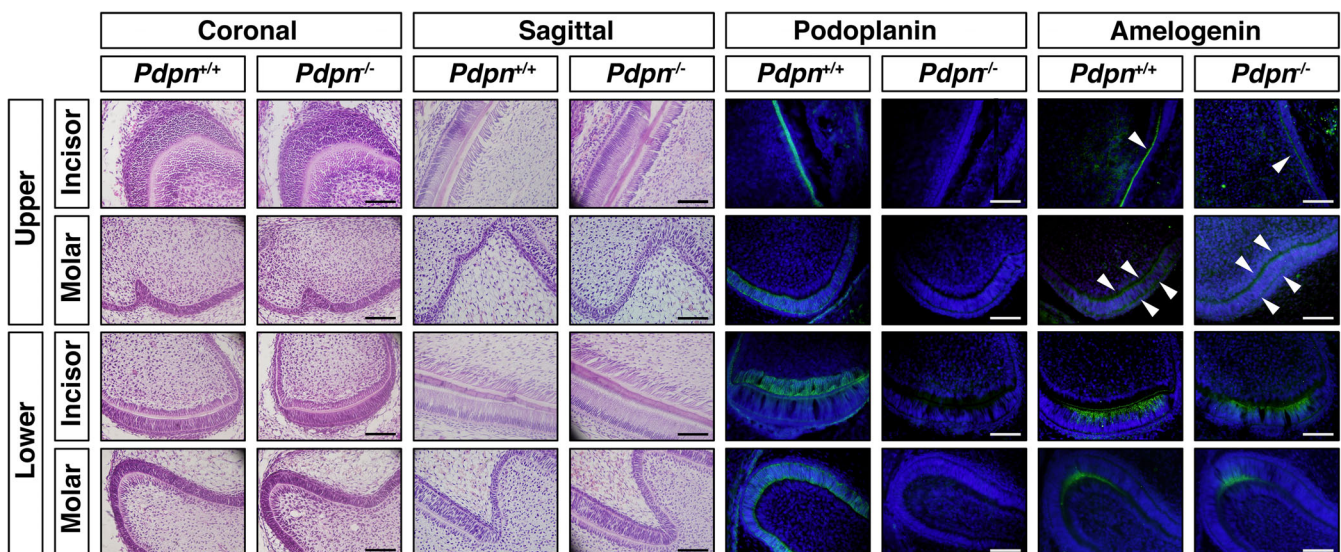


FIGURE 4 *Pdpr* mutant mice show normal amelogenesis and odontogenesis. Histologic observation and immunologic detection of podoplanin and amelogenin at E18.5. Coronal and sagittal paraffin sections (7 μ m) were made for upper and lower incisor and molar and stained with H&E. Similar sections were used for immunofluorescent detections for protein levels for podoplanin and amelogenin (arrowheads) for control (*Pdpr*^{+/+}) and homozygous null (*Pdpr*^{-/-}) mice. Bar = 50 μ m

TABLE 2 Ratio of genotyping of offspring from the breeding of mice carrying the Cre-recombined *Pdpn* allele

Background	Stage	Wildtype (%) <i>Pdpn</i> ^{+/+}	het (%) <i>Pdpn</i> ^{+/-}	Homo (%) <i>Pdpn</i> ^{-/-}	Total
129/B6	E18.5	25 (22.7)	54 (49.1)	31 (28.2)	110
129/B6	3 weeks	13 (25.5)	34 (66.7)	4 (7.8)	51
Swiss [#]	3 weeks	4 (16.7)	15 (62.5)	5 (20.8)	24

Abbreviation: #, backcrossed twice.

differences in collagen fibers as *Pdpn*^{-/-} mice showed mature collagen type1 fibers (Figure 3c). Also, there were no significant differences in Von Kossa stain (Figure 3c) between *Pdpn*^{-/-} mice and wildtype mice with regards to their calcified bone matrix. This result suggests that PDPN does not play critical role in skeletogenesis during embryogenesis.

Pdpn is expressed in enamel epithelial cells (Imaizumi et al., 2010). To characterize the tooth phenotype in these mice, we conducted histologic and immunostaining analyses at E18.5 (Figure 4). *Pdpn*^{-/-} mice did not show any tooth morphological changes; no significant differences in inner enamel epithelium, pre-dentin, or the odontoblasts layers (Figure 4, left). Polarization of ameloblasts was also observed in *Pdpn*^{-/-} mice. PDPN locates in the inner enamel epithelia, pre-dentin, and odontoblast layers of wild type mice. This result suggests that PDPN is produced from odontoblasts to inner enamel epithelia (Figure 4, right; Imaizumi et al., 2010). No immunosignal for PDPN further shows that the homozygous mice we generated here are null for *Pdpn* (Figure 4, right). To better understand the effect of loss of *Pdpn* in tooth bud development, we examined distribution of amelogenin, a marker for ameloblasts. However, no significant differences were observed in the incisor and molar between controls and mutants (Figure 4).

A limited number of homozygous mutant mice for the Cre-recombined allele (*Pdpn*^{-/-}) in 126S6/C57BL6 background survived for up to several months (Table 2). However, similar to the *Pdpn*^{fl/fl}; *Ocn*-Cre mice in the 126S6/C57BL6 background, approximately half of them showed smaller body size by 1 month after birth, with ascites. To address potential reasons for this pathologic condition, we examined the liver from the smaller *Pdpn*^{-/-} mice and compared to littermate controls (*Pdpn*^{+/+}) (Figure 5). Loss of PDPN signaling in *Pdpn*^{-/-} liver further confirmed that the mice are null for *Pdpn*. Reduced signal intensity for albumin suggests that a reduction in albumin in the serum may be responsible for the ascites. An increase of CD90 signal, a marker for developmental hepatic cells, in the mutant livers further supports the hypothesis that PDPN is important for normal differentiation of hepatocytes.

3.3 | Loss of *Pdpn* is compensated for in the Swiss outbred mouse background

Phenotypes from the same genetic manipulation can differ dramatically depending on mouse strain and genetic background (Mahtab et al., 2008; Mahtab et al., 2009). As mentioned earlier, we found that most of the homozygous mice for the floxed *Pdpn* allele (*Pdpn*^{fl/fl}) die at the perinatal stage likely due to lung malfunction (Table 1). When the mice were backcrossed to the Swiss outbred stock, the ratio of

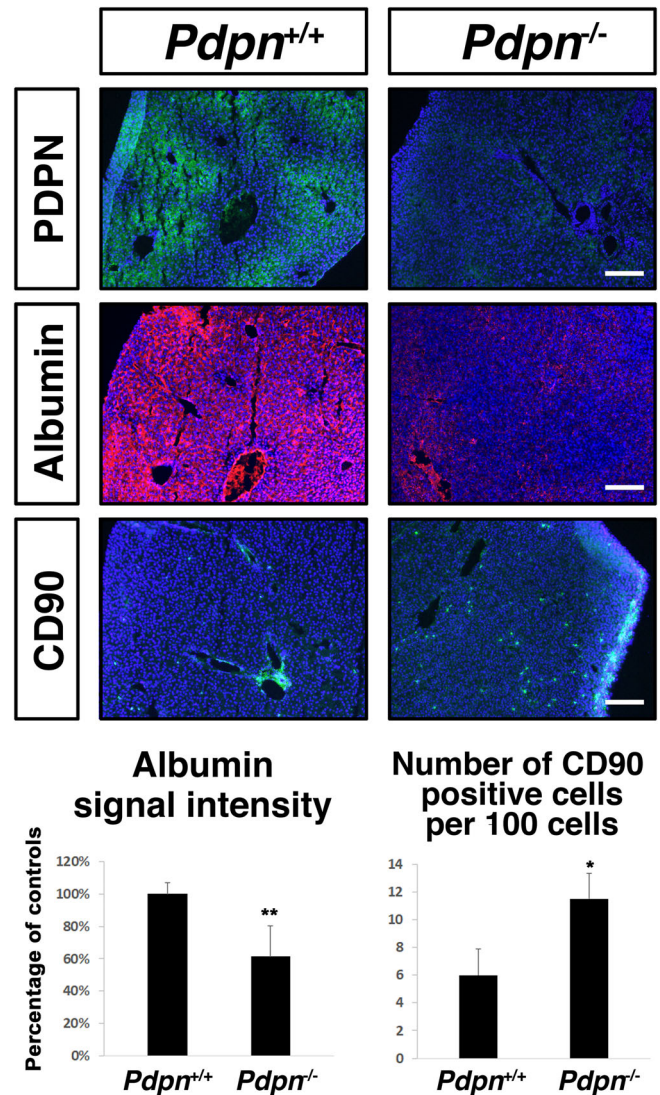


FIGURE 5 Surviving *Pdpn* mice in 126S6/C57BL6 mixed background showed liver abnormalities. Livers were removed from 5-week-old *Pdpn*^{+/-} and *Pdpn*^{-/-} mice and production of PDPN (green), albumin (red), and CD90 (green) were detected using cryosections. Intensity of immunosignals for albumin was quantified (20 cells for each genotype). Positive cells for CD90 were counted using two sections per liver (200 cells for each genotype). Bar = 50 μ m

homozygous mice for the floxed allele was significantly higher at 3 weeks of age compared to the 129/B6 background (Table 1). As expected, these mice did not show the presence of PDPN in kidney, lung, or bones (Figure 6). The normal survival rate suggested

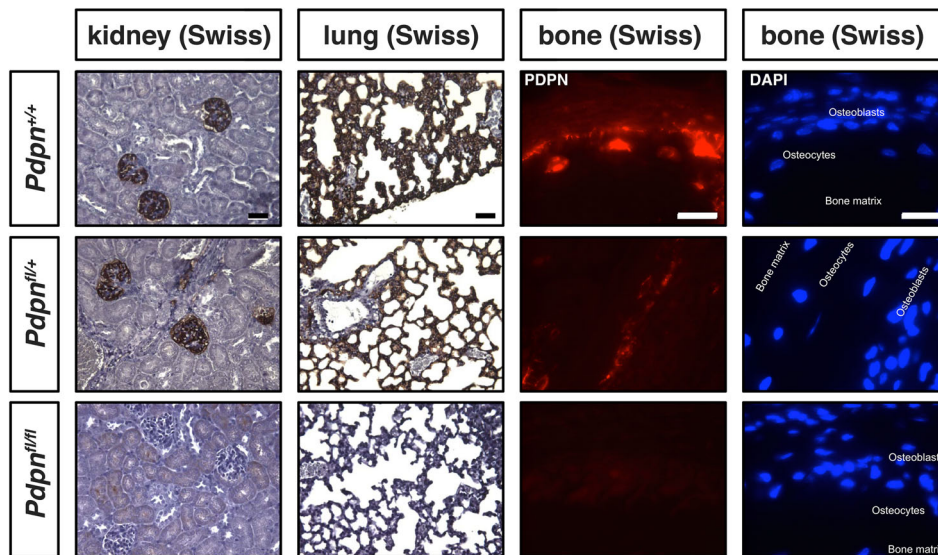


FIGURE 6 Homozygous floxed *Pdpn* mice in Swiss background survived without PDPN protein. Presence of PDPN was detected using sections from kidney, lung, and bones prepared from Swiss background in wildtype but not null animals. Immunoseignals were visualized by peroxidase reaction (kidney and lung) or a secondary antibody conjugated with Cy3 (bone, red). Bar = 20 μ m

compensation by another gene(s). This interpretation is further supported by the observation that homozygous mice for Cre-recombined allele (*Pdpn*^{-/-}) can survive to the age of 3 weeks with expected Mendelian ratios after twice of backcrossing with Swiss outbred mice (Table 2).

Since *Pdpn* is highly expressed in early osteocytes, we looked at osteocyte lacunar morphology in the tibia of 6-month-old mice in the Swiss outbred background (backcrossed twice or more, 75% or more was Swiss background). X-ray images from tibia, calvaria, and lumbar vertebrae did not show any significant differences between control (*Pdpn*^{+/-}) and homozygous mutant mice (*Pdpn*^{-/-}) (Figure 7a-c). Acid-etching did not reveal any overt differences in shape and number of osteocyte lacunae or canaliculi (Figure 7d). After exercise of 4-month-old animals of the Swiss outbred background, no overt differences were noted between exercised control and the exercised mutant groups (*Pdpn*^{-/-}, 75% or more was Swiss background) (Figure 7e).

4 | DISCUSSION

Here, we show that PDPN can be dispensable or indispensable depending on the mouse genetic background. Our newly developed 129/B6 murine model carrying floxed alleles for podoplanin (*Pdpn*^{fl/fl}) showed significant perinatal lethality and those that survived showed severe hypomorphism. The surviving homozygous mutant mice in 129/B6 mixed background showed reduced numbers of canaliculi in osteocytes and increased trabecular bone volume. Homozygous mice for the Cre-recombined allele (*Pdpn*^{-/-}) die perinatally due to insufficient lung development as previously reported, but no overt changes were observed in the skeletal system including long bones and teeth. Hepatic malfunctions were found in surviving *Pdpn* floxed or null allele in the 129/B6 mixed background resulting in small size and ascites production. Surprisingly, this perinatal lethality does not occur with global deletion of *Pdpn* in the Swiss outbred background. Homozygous null mice (*Pdpn*^{-/-}) in the Swiss background did not show any

overt bone phenotype or changes in osteocyte lacunocanicular network nor an atypical response to exercise. These data suggest that unknown changes in gene expression may compensate for the loss of *Pdpn* in the Swiss background and that they may make PDPN be completely dispensable for physiologic skeletal formation and responses to the mechanoenvironment.

There are several reports using conditional mouse models for *Pdpn*. In a conditional mouse line floxing exon 3 of *Pdpn* crossed with an *Osteocalcin*-Cre mouse line, dendrite volume and length were significantly reduced in 6-week-old mutant mice (Staines et al., 2017). This is in contrast to our data showing no overt changes in the length of canaliculi, suggesting that if loss of PDPN was compensated for during development, it would no longer be required for bone homeostasis. It is reported that PDPN levels in osteocytes are increased in osteoarthritic subchondral bones from humans, canines, and mice (Staines et al., 2019). Conditional mutant mice for *Pdpn* showed resistance against load-induced osteoarthritis, suggesting that PDPN is involved in the pathogenesis of osteoarthritis (Staines et al., 2019). Mice with bone cell-specific disruption of *Pdpn* showed resistance to ovariectomy-induced bone loss (Staines et al., 2020). Interestingly, the increase in osteoclast activity due to ovariectomy was suppressed in the mutant mice despite alterations in the RANKL/OPG ratio, suggesting that PDPN plays a role in osteoblasts/osteocytes to support osteoclastogenesis through a mechanism independent of the RANKL/OPG axis (Staines et al., 2020). These data suggest that PDPN functions in bone cells to positively regulate osteoclast function, which could be one of the reasons of the increased trabecular bone mass in our *Pdpn* mutant mice in the mixed background. In contrast to our studies and the studies by Staines and colleagues, there is no overt tooth phenotype observed in 2-week-old *Pdpn* conditional mice using the neural crest-specific *Wnt1*-Cre line (Takara et al., 2017).

Initially, we aimed to develop a conditional mutant allele for *Pdpn* by floxing exon 1. We soon realized that homozygous mice for the floxed-neo allele resulted in perinatal lethality. Removal of the

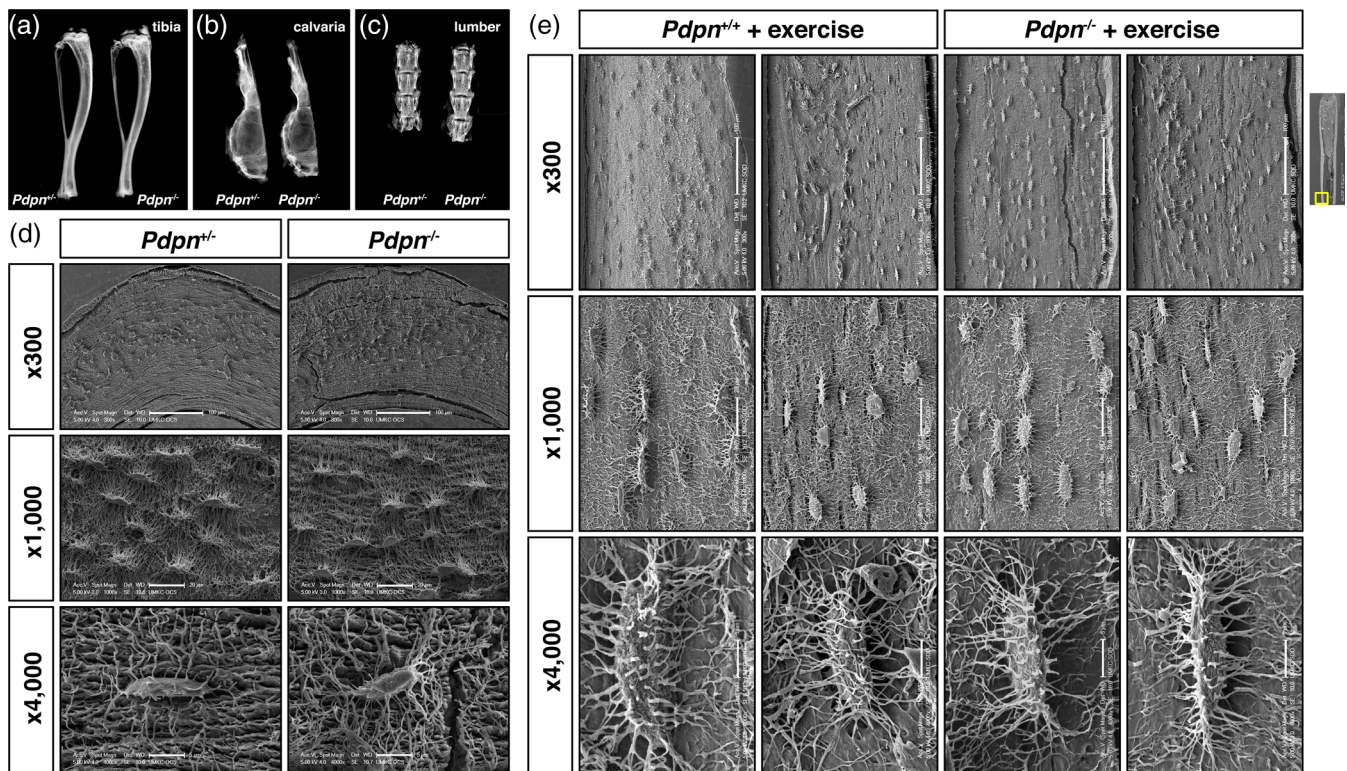


FIGURE 7 Homozygous null *Pdpn* mice in Swiss background did not show any overt bone phenotypes. (a–c) X-ray radiograms of indicated bones from control (*Pdpn*^{+/+}) and homozygous mutant mice (*Pdpn*^{-/-}) at 6 months of age. (d) Electron microscopy of acid-etched resin embedded bone shows the density and morphology of osteocyte lacunae and canaliculi in the cortical compartments of tibia. (e) *Pdpn*^{+/+} and *Pdpn*^{-/-} mice were exercised on a treadmill for 3 weeks and morphology of osteocyte lacunae and canaliculi were revealed using electron microscopy of acid-etched resin embedded bone. The midshaft area of femoral cortical compartments was used as indicated as a yellow box on the right most panel

neomycin cassette from the targeted allele did not improve the lethality. Taking these data together, these results suggest that insertion of a loxP site in the 5'-UTR of exon 1 may result in lower expression of *Pdpn* expression or reduced stability of *Pdpn* mRNA. We found significant improvement in neonatal lethality after twice back-crossing to the Swiss outbred background, when theoretically 75% of the genome is replaced by the Swiss background. This is far less than the 5–10 back-crosses needed to produce a congenic strain. The homozygous mice in the Swiss background, which escape from lethality, still do not produce PDPN protein suggesting that these mutant mice are rescued, not because changes in *Pdpn* mRNA, but because other genes compensate for a lack of PDPN in the mutants. We are presently screening differentially expressed genes that could explain the compensation for lethality and the bone phenotype found in surviving *Pdpn* mutant mice. Candidate genes may include MT1-MMP, which is required for osteocyte processes (Holmbeck et al., 2005), and destrin, which is involved in cytoskeletal rearrangement (Guo et al., 2010).

Taken together, the conditional gene knockout approach reveals important functions of PDPN in skeletal homeostasis, but if early lethality is rescued in a different genetic background (Swiss outbred stock in this case), the rescued mice do not show any overt skeletal phenotypes even after application of mechanical loading. We hypothesize that some genes are upregulated (or downregulated) in the rescued mutant mice for *Pdpn* to compensate for the loss of PDPN,

especially during type 1 cell differentiation in the lung, and that the rescued mice develop a skeletal system that no longer requires PDPN for its homeostasis. Of note, there are no known structurally related genes to PDPN. Identifying differentially expressed genes in the rescued mutant mice would be an important future direction to deepen our understanding of skeletal homeostasis.

ACKNOWLEDGEMENT

The authors thank Dr. Andrew Farr for E11 antibody, Dr. Tarak Srivastava and Mr. Michael Falzon for contribution of immunodetection experiments on kidney/lung and liver, respectively. The authors thank Ms. Hong Zhao and Yixia Anita Xie for excellent technical support. The authors also thank Drs. Vladimir Dusevich for SEM, David Valentin for microCT, Mark Dallas for osteocyte analyses and Koki Nagano for treadmill operations. This study is supported by the National Institutes of Health (R01DE020843 to Y.M., R03DE027456 to H.Z., R01DE024797 to S.E.H., and P01AG39355 to L.F.B.). The molecular biology core at the School of Dentistry is funded by NIH/P30AR069620. M.T.N. is funded by Fukuoka Dental College Foreign Exchange Program.

AUTHOR CONTRIBUTIONS

Study design: M.T.N., H.Z., D.G., J.Q.F., L.F.B., and Y.M. Materials to generate: D.G., G.S., M.H., M.R., S.E.H., and Y.M. Study conduct, data

collection, and data analysis: M.T.N., H.Z., D.G., H.U., H.P., and Y.M. Data interpretation: M.T.N., H.Z., D.G., S.E.H., J.Q.F., L.F.B., and Y.M. Writing manuscript: M.T.N., H.Z., D.U., L.F.B., and Y.M. All authors approved final version of manuscript. H.Z. and Y.M. take responsibility for the integrity of the data analysis.

DATA AVAILABILITY STATEMENT

The data that support the findings of this study are available from the corresponding author upon reasonable request.

ORCID

Masako Toda Nakamura  <https://orcid.org/0000-0002-1588-5388>

Yuji Mishina  <https://orcid.org/0000-0002-6268-4204>

REFERENCES

- Amano, I., Imaizumi, Y., Kaji, C., Kojima, H., & Sawa, Y. (2011). Expression of podoplanin and classical cadherins in salivary gland epithelial cells of klotho-deficient mice. *Acta Histochemica et Cytochemica*, *44*, 267–276.
- Astarita, J. L., Acton, S. E., & Turley, S. J. (2012). Podoplanin: Emerging functions in development, the immune system, and cancer. *Frontiers in Immunology*, *3*, 283.
- Bonewald, L. F. (2011). The amazing osteocyte. *Journal of Bone and Mineral Research*, *26*, 229–238.
- Farley, F. W., Soriano, P., Steffen, L. S., & Dymecki, S. M. (2000). Widespread recombinase expression using FLPeR (flipper) mice. *Genesis*, *28*, 106–110.
- Gonzalez, R. F., & Dobbs, L. G. (1998). Purification and analysis of RT140, a type I alveolar epithelial cell apical membrane protein. *Biochimica et Biophysica Acta*, *1429*, 208–216.
- Groger, M., Loewe, R., Holnthoner, W., Embacher, R., Pillinger, M., Herron, G. S., ... Petzelbauer, P. (2004). IL-3 induces expression of lymphatic markers Prox-1 and podoplanin in human endothelial cells. *Journal of Immunology*, *173*, 7161–7169.
- Guo, D., Keightley, A., Guthrie, J., Veno, P. A., Harris, S. E., & Bonewald, L. F. (2010). Identification of osteocyte-selective proteins. *Proteomics*, *10*, 3688–3698.
- Hayashi, S., Tenzen, T., & McMahon, A. P. (2003). Maternal inheritance of Cre activity in a Sox2Cre deleter strain. *Genesis*, *37*, 51–53.
- Holmbeck, K., Bianco, P., Pidoux, I., Inoue, S., Billingham, R. C., Wu, W., ... Poole, A. R. (2005). The metalloproteinase MT1-MMP is required for normal development and maintenance of osteocyte processes in bone. *Journal of Cell Science*, *118*, 147–156.
- Imaizumi, Y., Amano, I., Tsuruga, E., Kojima, H., & Sawa, Y. (2010). Immunohistochemical examination for the distribution of podoplanin-expressing cells in developing mouse molar tooth germs. *Acta Histochemica et Cytochemica*, *43*, 115–121.
- Iura, A., McNerny, E. G., Zhang, Y., Kamiya, N., Tantillo, M., Lynch, M., ... Mishina, Y. (2015). Mechanical loading synergistically increases trabecular bone volume and improves mechanical properties in the mouse when BMP signaling is specifically ablated in osteoblasts. *PLoS One*, *10*, e0141345.
- Mahtab, E. A., Vicente-Steijn, R., Hahurij, N. D., Jongbloed, M. R., Wisse, L. J., DeRuiter, M. C., ... Gittenberger-de Groot, A. C. (2009). Podoplanin deficient mice show a RhoA-related hypoplasia of the sinus venosus myocardium including the sinoatrial node. *Developmental Dynamics*, *238*, 183–193.
- Mahtab, E. A., Wijffels, M. C., Van Den Akker, N. M., Hahurij, N. D., Lie-Venema, H., Wisse, L. J., ... Gittenberger-De Groot, A. C. (2008). Cardiac malformations and myocardial abnormalities in podoplanin knockout mouse embryos: Correlation with abnormal epicardial development. *Developmental Dynamics*, *237*, 847–857.
- Martin-Villar, E., Fernandez-Munoz, B., Parsons, M., Yurrita, M. M., Megias, D., Perez-Gomez, E., ... Quintanilla, M. (2010). Podoplanin associates with CD44 to promote directional cell migration. *Molecular Biology of the Cell*, *21*, 4387–4399.
- Noda, Y., Amano, I., Hata, M., Kojima, H., & Sawa, Y. (2010). Immunohistochemical examination on the distribution of cells expressed lymphatic endothelial marker podoplanin and LYVE-1 in the mouse tongue tissue. *Acta Histochemica et Cytochemica*, *43*, 61–68.
- Prideaux, M., Dallas, S. L., Zhao, N., Johnsrud, E. D., Veno, P. A., Guo, D., ... Bonewald, L. F. (2015). Parathyroid hormone induces bone cell motility and loss of mature osteocyte phenotype through L-calcium channel dependent and independent mechanisms. *PLoS One*, *10*, e0125731.
- Prideaux, M., Loveridge, N., Pitsillides, A. A., & Farquharson, C. (2012). Extracellular matrix mineralization promotes E11/gp38 glycoprotein expression and drives osteocytic differentiation. *PLoS One*, *7*, e36786.
- Ramirez, M. I., Millien, G., Hinds, A., Cao, Y., Seldin, D. C., & Williams, M. C. (2003). T1alpha, a lung type I cell differentiation gene, is required for normal lung cell proliferation and alveolus formation at birth. *Developmental Biology*, *256*, 61–72.
- Renart, J., Carrasco-Ramirez, P., Fernandez-Munoz, B., Martin-Villar, E., Montero, L., Yurrita, M. M., & Quintanilla, M. (2015). New insights into the role of podoplanin in epithelial-mesenchymal transition. *International Review of Cell and Molecular Biology*, *317*, 185–239.
- Retzbach, E. P., Sheehan, S. A., Nevel, E. M., Batra, A., Phi, T., Nguyen, A. T. P., ... Goldberg, G. S. (2018). Podoplanin emerges as a functionally relevant oral cancer biomarker and therapeutic target. *Oral Oncology*, *78*, 126–136.
- Sawa, Y., Iwasawa, K., & Ishikawa, H. (2008). Expression of podoplanin in the mouse tooth germ and apical bud cells. *Acta Histochemica et Cytochemica*, *41*, 121–126.
- Schacht, V., Ramirez, M. I., Hong, Y. K., Hirakawa, S., Feng, D., Harvey, N., ... Detmar, M. (2003). T1alpha/podoplanin deficiency disrupts normal lymphatic vasculature formation and causes lymphedema. *The EMBO Journal*, *22*, 3546–3556.
- Schulze, E., Witt, M., Kasper, M., Lowik, C. W., & Funk, R. H. (1999). Immunohistochemical investigations on the differentiation marker protein E11 in rat calvaria, calvaria cell culture and the osteoblastic cell line ROS 17/2.8. *Histochemistry and Cell Biology*, *111*, 61–69.
- Staines, K. A., Hopkinson, M., Dillon, S., Stephen, L. A., Fleming, R., Sophocleous, A., ... Farquharson, C. (2020). Conditional deletion of E11/Podoplanin in bone protects against ovariectomy-induced increases in osteoclast formation and activity. *Bioscience Reports*, *40*. <https://doi.org/10.1042/BSR20190329>
- Staines, K. A., Ikpegbu, E., Tornqvist, A. E., Dillon, S., Javaheri, B., Amin, A. K., ... Farquharson, C. (2019). Conditional deletion of E11/podoplanin in bone protects against load-induced osteoarthritis. *BMC Musculoskeletal Disorders*, *20*, 344.
- Staines, K. A., Javaheri, B., Hohenstein, P., Fleming, R., Ikpegbu, E., Unger, E., ... Farquharson, C. (2017). Hypomorphic conditional deletion of E11/Podoplanin reveals a role in osteocyte dendrite elongation. *Journal of Cellular Physiology*, *232*, 3006–3019.
- Suzuki-Inoue, K., Osada, M., & Ozaki, Y. (2017). Physiologic and pathophysiological roles of interaction between C-type lectin-like receptor 2 and podoplanin: Partners from in utero to adulthood. *Journal of Thrombosis and Haemostasis*, *15*, 219–229.
- Takara, K., Maruo, N., Oka, K., Kaji, C., Hatakeyama, Y., Sawa, N., ... Sawa, Y. (2017). Morphological study of tooth development in podoplanin-deficient mice. *PLoS One*, *12*, e0171912.
- Zhang, K., Barragan-Adjemian, C., Ye, L., Kotha, S., Dallas, M., Lu, Y., ... Bonewald, L. F. (2006). E11/gp38 selective expression in osteocytes: Regulation by mechanical strain and role in dendrite elongation. *Molecular and Cellular Biology*, *26*, 4539–4552.
- Zhao, M., Xiao, G., Berry, J. E., Franceschi, R. T., Reddi, A., & Somerman, M. J. (2002). Bone morphogenetic protein 2 induces dental follicle cells to differentiate toward a cementoblast/osteoblast phenotype. *Journal of Bone and Mineral Research*, *17*, 1441–1451.

Zhao, N., Nociti, F. H., Jr., Duan, P., Prideaux, M., Zhao, H., Foster, B. L., ... Bonewald, L. F. (2016). Isolation and functional analysis of an immortalized murine cementocyte cell line, IDG-CM6. *Journal of Bone and Mineral Research*, 31, 430–442.

SUPPORTING INFORMATION

Additional supporting information may be found in the online version of the article at the publisher's website.

How to cite this article: Toda Nakamura, M., Zhang, H., Guo, D., Ueharu, H., Pan, H., Scott, G., Harris, M., Ray, M., Feng, J. Q., Harris, S. E., Bonewald, L. F., & Mishina, Y. (2021). Podoplanin is dispensable for mineralized tissue formation and maintenance in the Swiss outbred mouse background. *genesis*, 59(10), e23450. <https://doi.org/10.1002/dvg.23450>